Supplemental Material

Recent climate variability around the Kerguelen Islands (Southern Ocean) seen through weather regimes
— Supplementary Materials —

Journal of Climate https://doi.org/10.1175/JCLI-D-20-0255.1

Benjamin Pohl; Thomas Saucède; Vincent Favier; Julien Pergaud;
Deborah Verfaillie; Ylber Krasniqi; Yves Richard

In the Supplementary Materials below, we present figures that could not appear in the main paper to keep it concise. They could yet be useful to some readers.

First, we present results that are only briefly discussed in the main paper. This is the case for the red-noise test allowing for an objective choice of the number of clusters to be retained (Supp. Fig. 1), the seasonality and interannual distribution of regime occurrence (Supp. Fig. 2) or the time persistence of the regime sequences (Supp. Fig. 3), and the hemispheric-scale Z_{700} anomalies during the regime occurrences (Supp. Figs. 10-12). Similarly, the annual cycle of atmospheric and oceanic variables recorded at various locations on Kerguelen are presented in Supp. Figs. 15, 18, 20, 21.
In order to better understand how regimes modulate temperature and precipitation over the Southern Ocean and Kerguelen Islands, we also show in Supp. Figs. 8 and 9 the anomalies of total cloud cover in the air column, total water in the air column, and vertical velocity of the wind at 850 and 500hPa. These analyses, performed over the whole period 1979-2018 and for all months of the year, help assess how atmospheric instability is modulated by the regimes, in time and space.

Most remaining analyses presented below address the seasonal-dependency of our results, an issue that is discussed throughout the paper since we defined our weather regimes for the whole year, but that could not always be shown as main figures.
Some figures of the main paper only present results for the whole period, or a single season (e.g. the austral summer season), but do not show seasonal declinations of these analyses. The materials presented below help fill this gap. This is for instance the case for Supp. Figs. 10-11, showing relationship between weather regimes and large-scale background climate conditions in winter (as Figs. 8-9 do for summer in the article), or Supp. Figs. 15-16, 18-19 and 21, presenting spatial contrasts in atmospheric and oceanic variables in Kerguelen.
Similarly, Supplementary Figures 4 and 5 that respectively present seasonal mean composites of Z_{500}, wind at 850 hPa and 2-m air temperature during regime occurrence but during the summer and winter seasons, instead of the whole year. The same approach is used for specific humidity and surface shortwave radiative anomalies (Supp. Figs. 7-8), since only year-round composites are considered in the main paper.

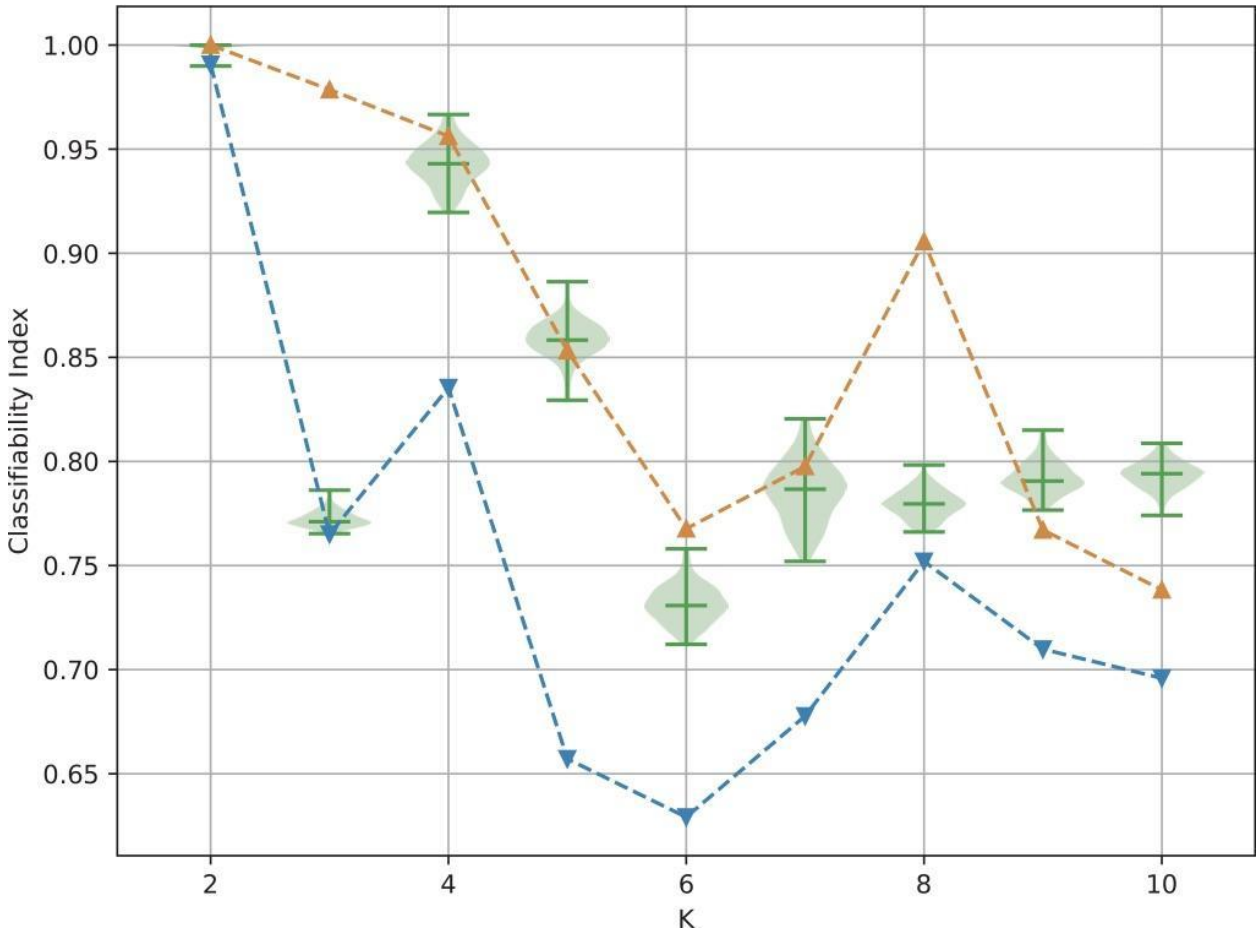

Supplementary Figure 1 | Spread of the classifiability index as a function of the number of regimes K for 100 clusterings initialized with different random draws. The levels of significance at 5 and 95% (resp. blue line with lower triangles, and orange line with upper triangles) are computed according to a first-order Markov process (also known as “red-noise test”).

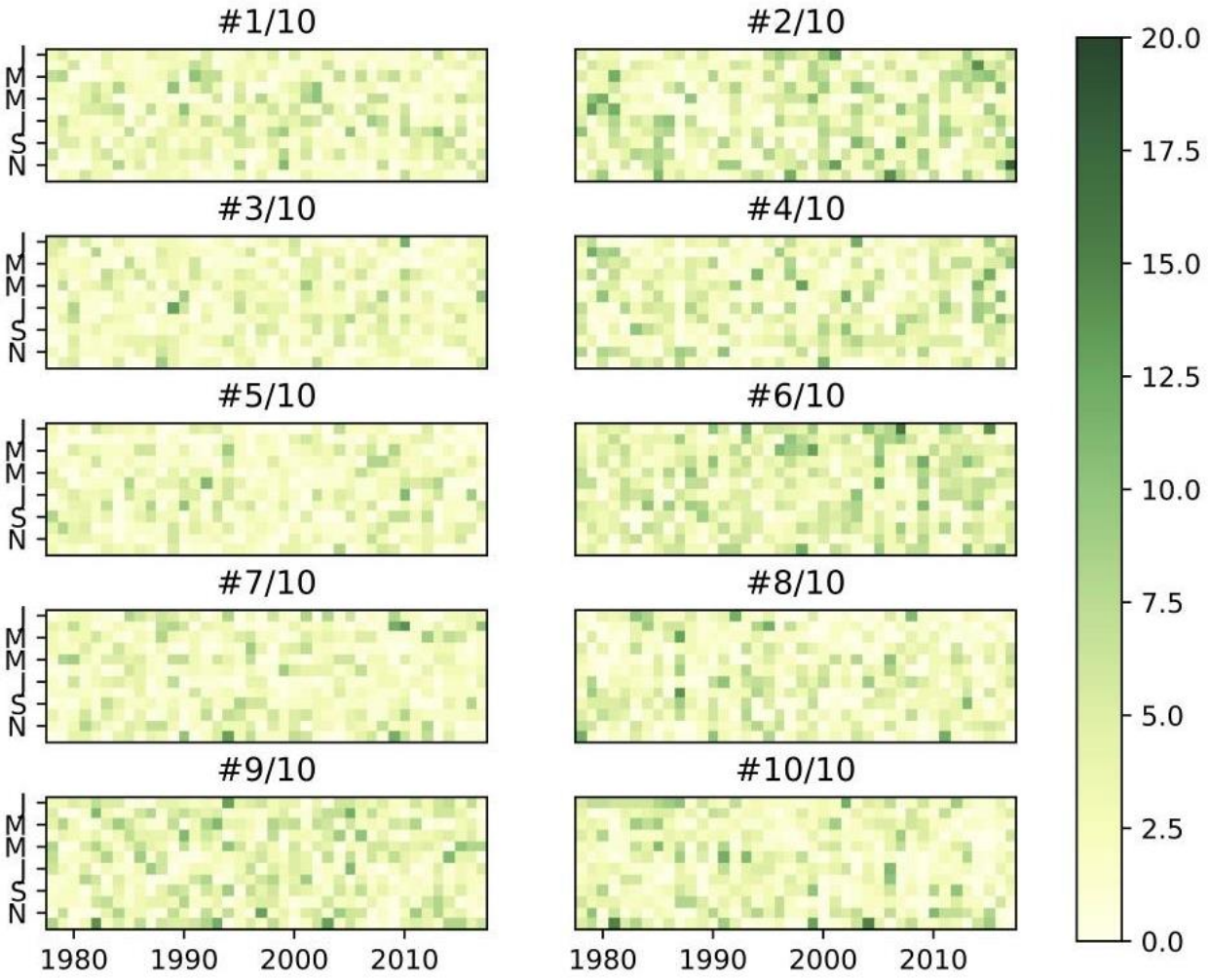

Supplementary Figure 2 | Number of occurrences of each regime during each month (y-axis) of the 1979-2018 period (x-axis), see color legend.

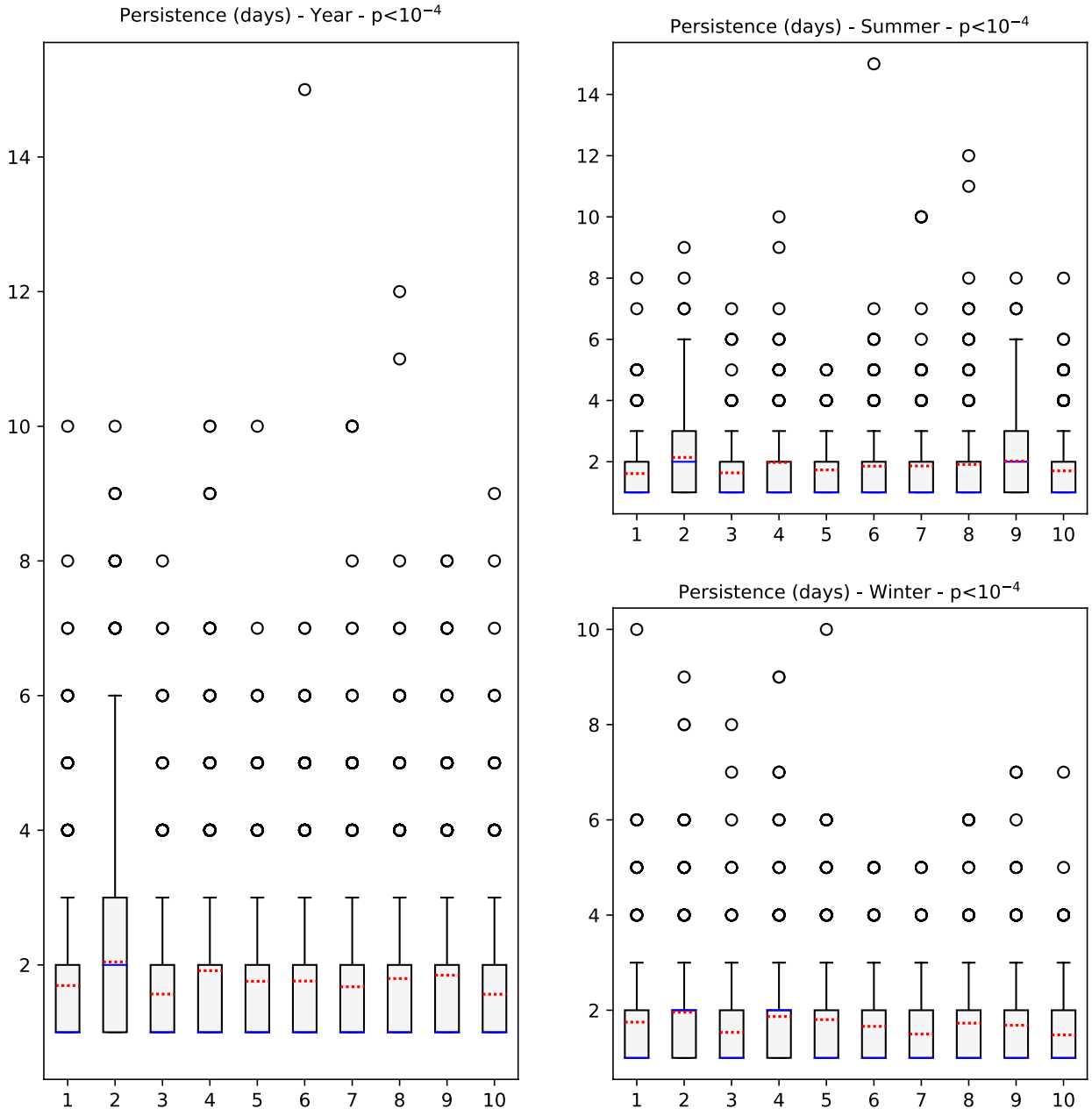

Supplementary Figure 3 | Box-and-whisker representation of the persistence of regime sequences. The left-hand panel is for the whole period. Right-hand panels are for austral summer (NDJF) and winter (JJAS) seasons. Statistical significance is tested as in Fig. 10. The boxes have lines at the lower quartile, median (blue line) and upper quartile values. The average is shown by the dashed red lines. The whiskers are lines extending from each end of the box up to the 1.5 interquartile range. Outliers (beyond the 1.5 interquartile range) are represented as lack circles. In order to avoid splitting sequences because of inter-member uncertainties, the zero category is here omitted and all analyses are carried out for regimes derived from the first member of ERA5.

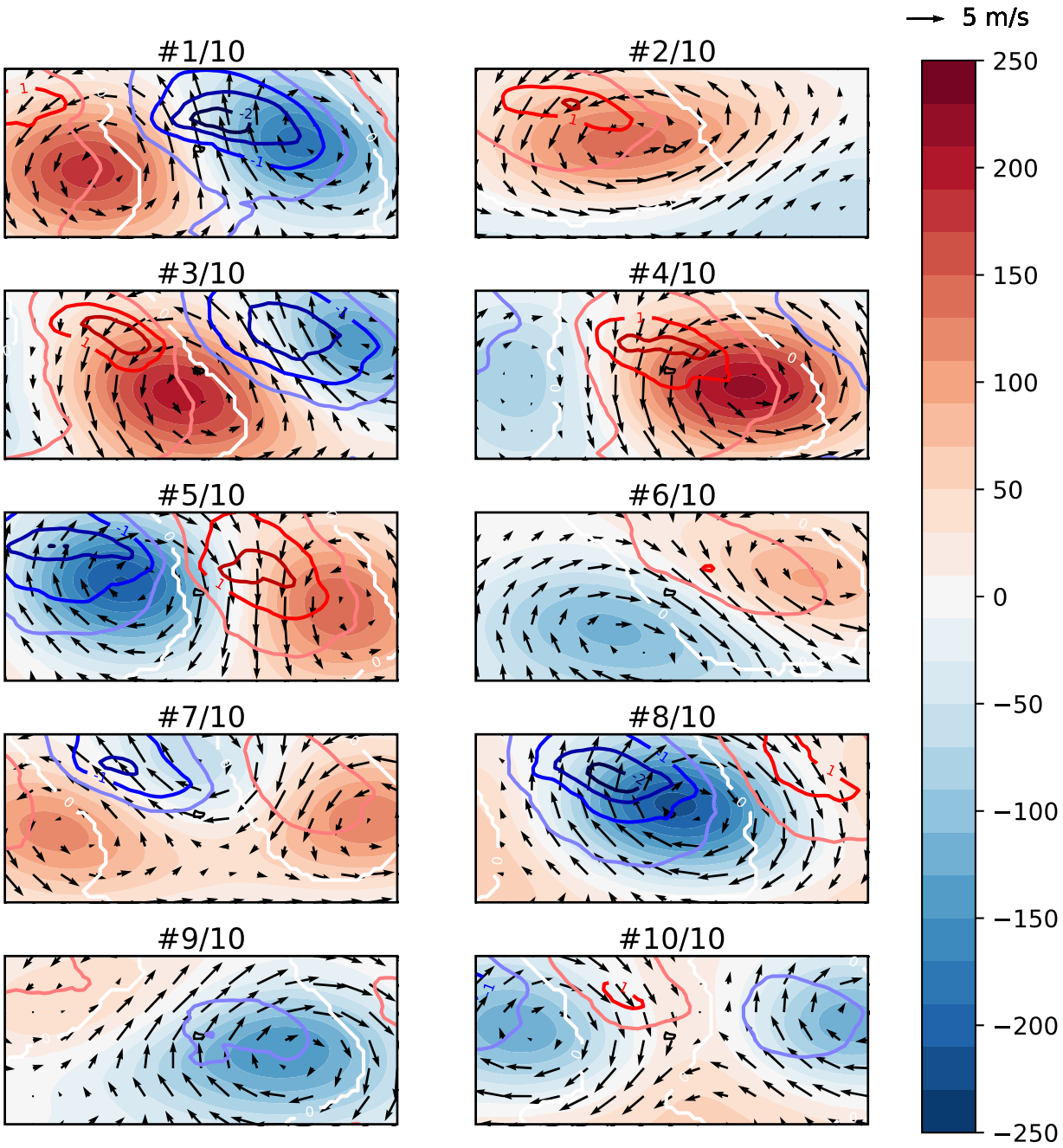

Supplementary Figure 4 | As Fig. 6 but for the austral summer season (NDJF).

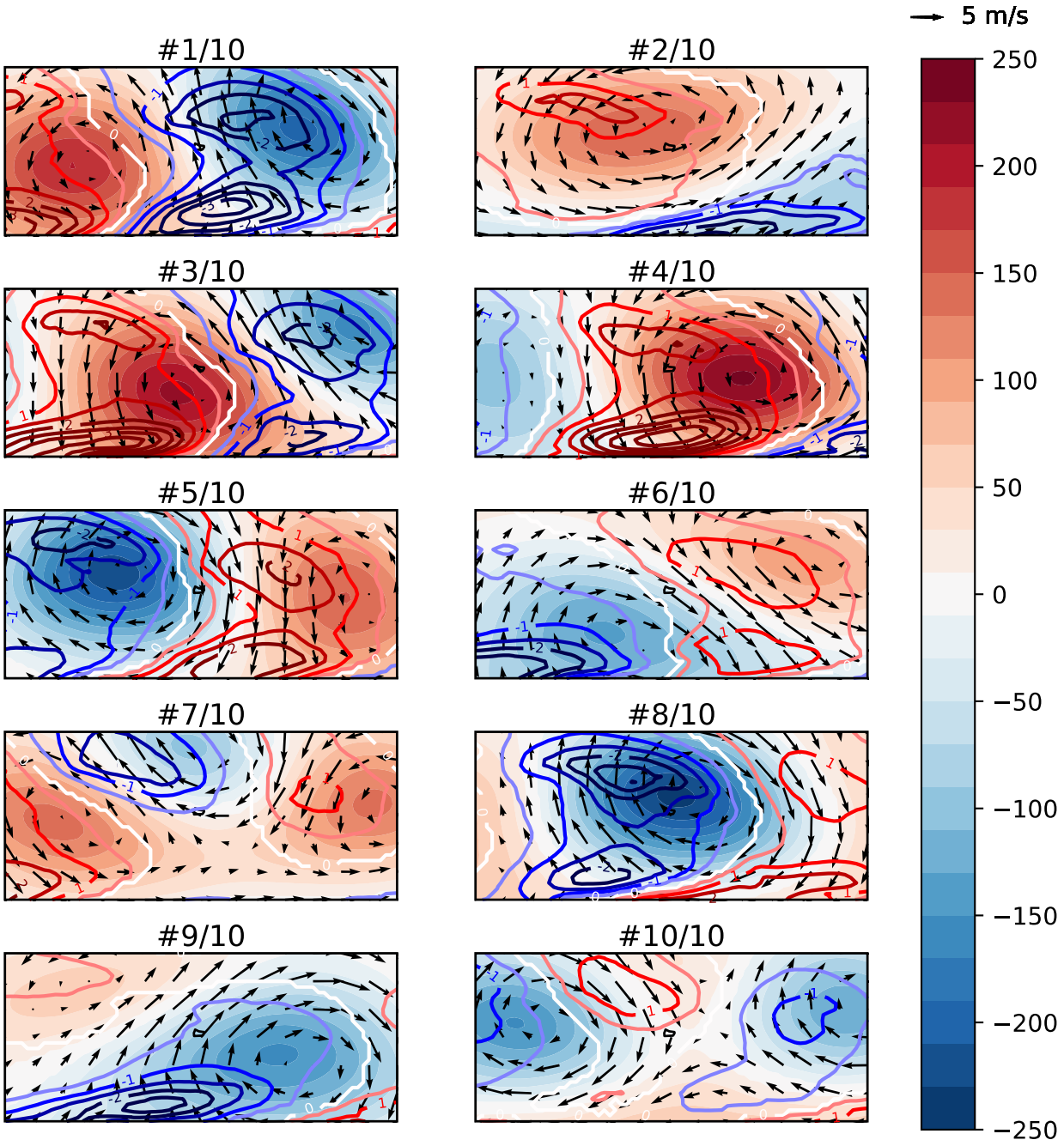

Supplementary Figure 5 | As Fig. 6 but for the austral winter season (JJAS).

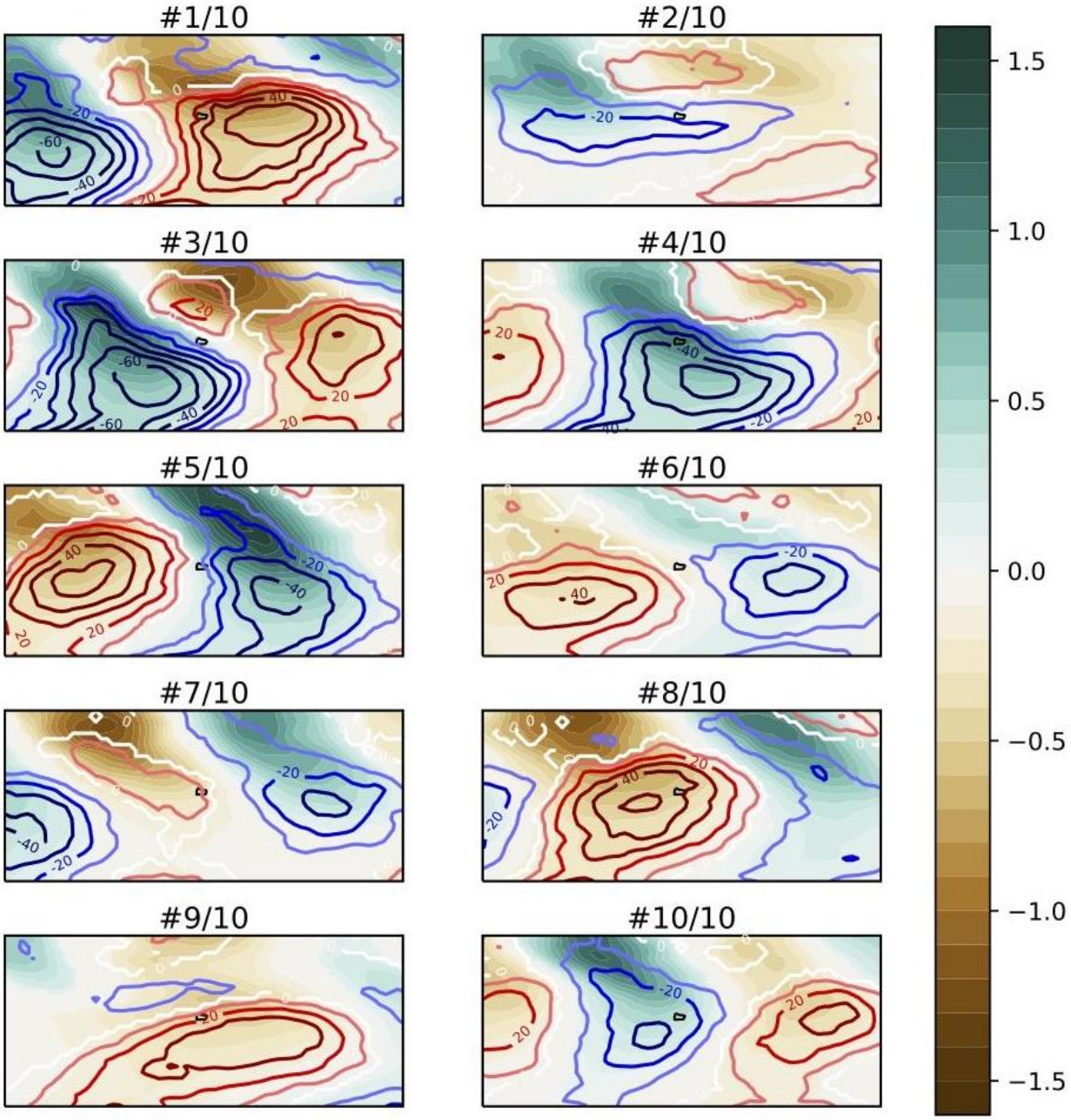

Supplementary Figure 6 | As Fig. 7 but for the austral summer season (NDJF).

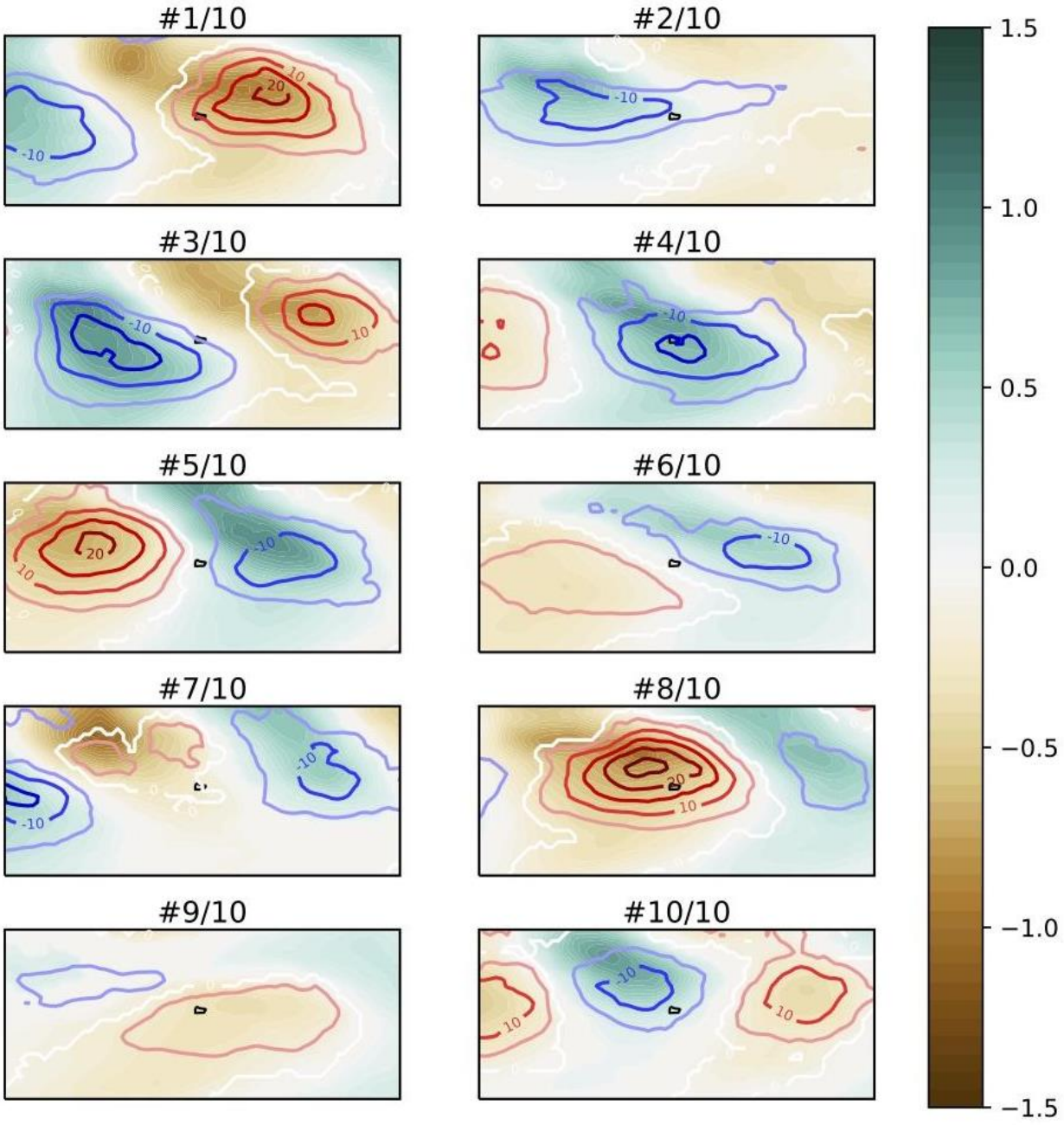

Supplementary Figure 7 | As Fig. 7 but for the austral winter season (JJAS).

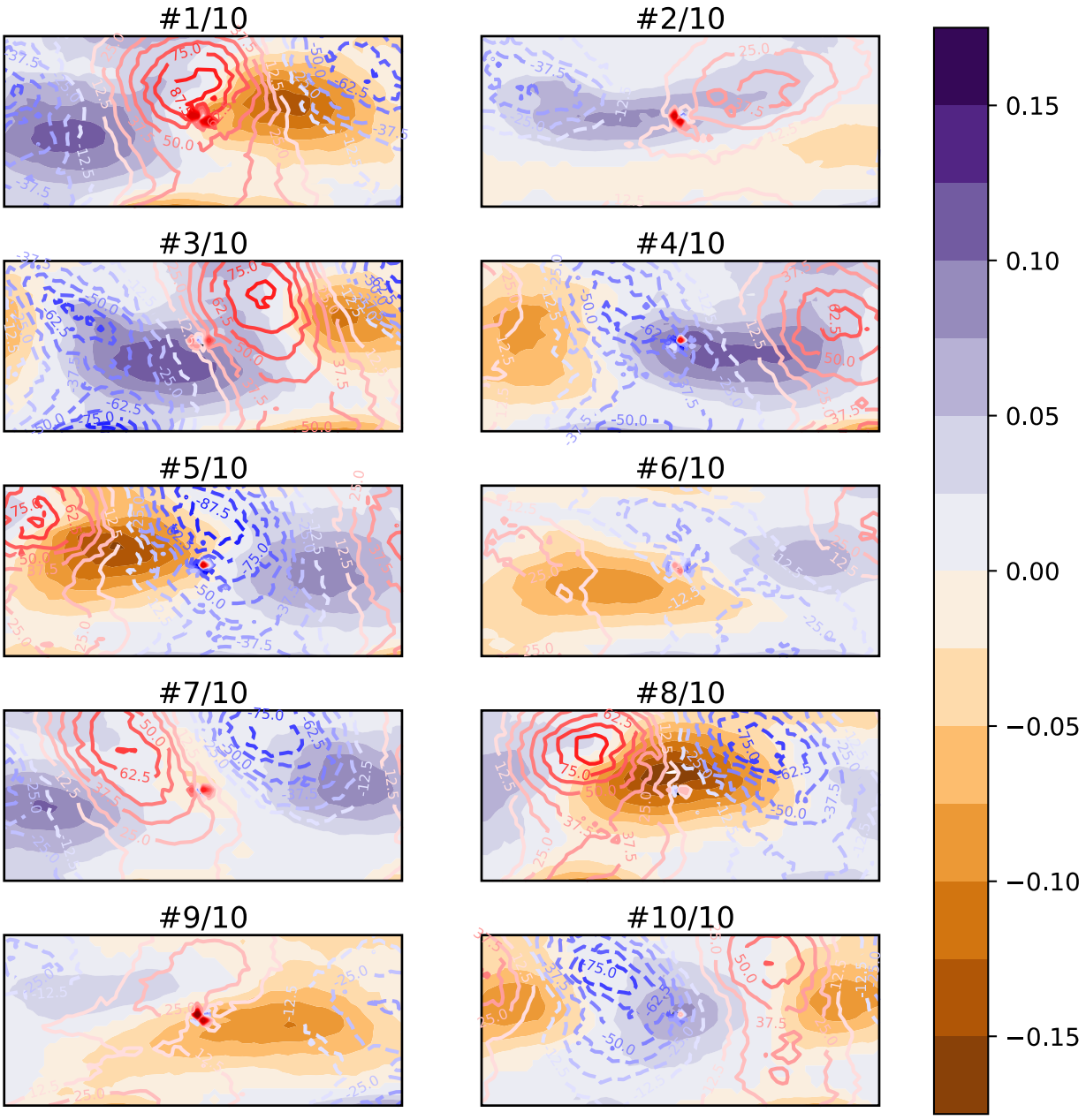

Supplementary Figure 8 | As Fig. 6 but for synchronous anomalies of total cloud cover over the air column (fraction, see color legend) and vertical velocity at 500hPa (x10^3 Pa.s^{-1}, contours). Contour equidistance is 12.5x10^3 Pa.s^{-1}, with the zero isoline omitted.

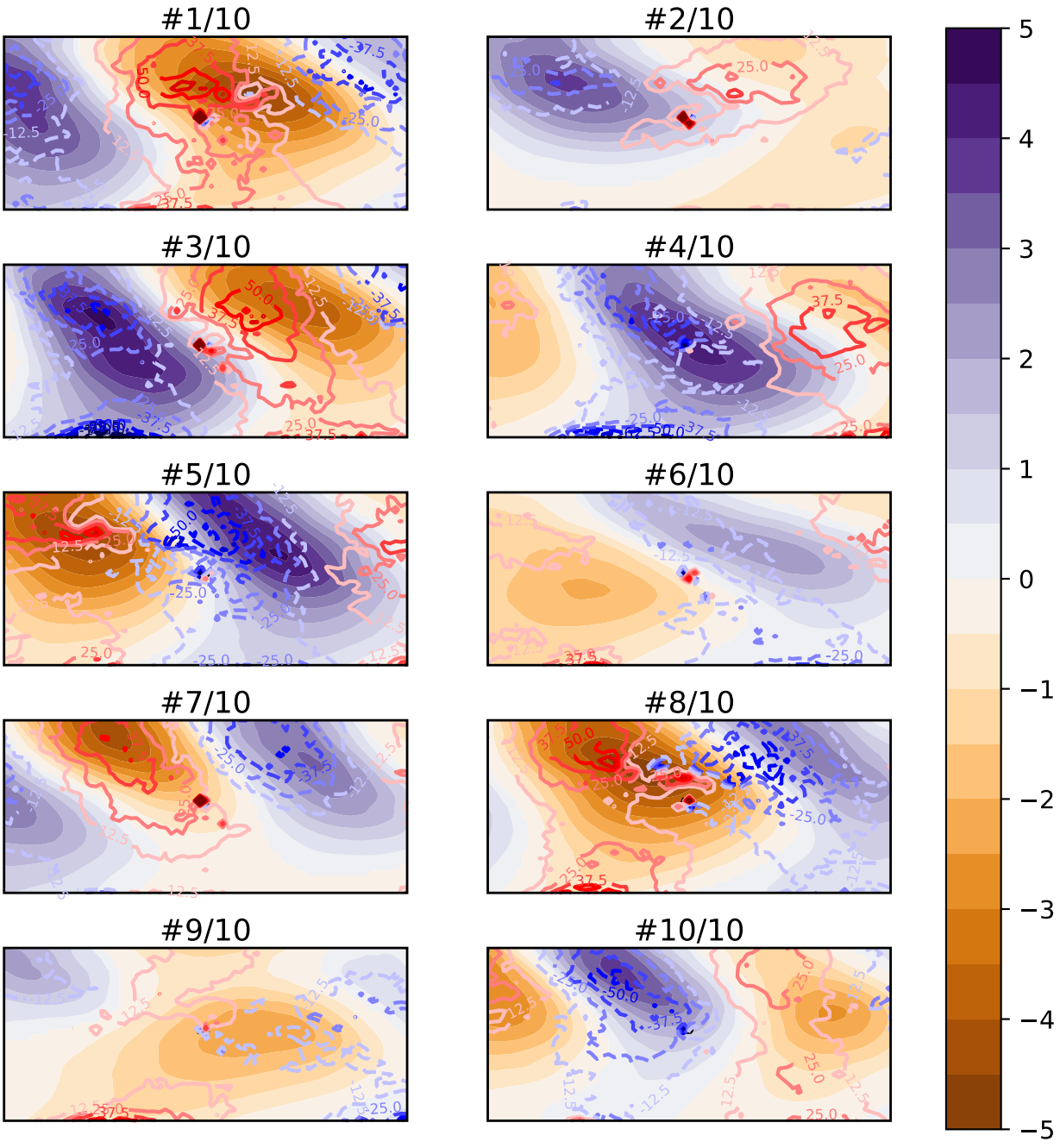

Supplementary Figure 9 | As Fig. 6 but for anomalies of total water content of the air column (kg.m^{-2}, see color legend) and vertical velocity at 850hPa (x10^{3} Pa.s^{-1}, contours). Contour equidistance is 12.5x10^{3} Pa.s^{-1}, with the zero isoline omitted.

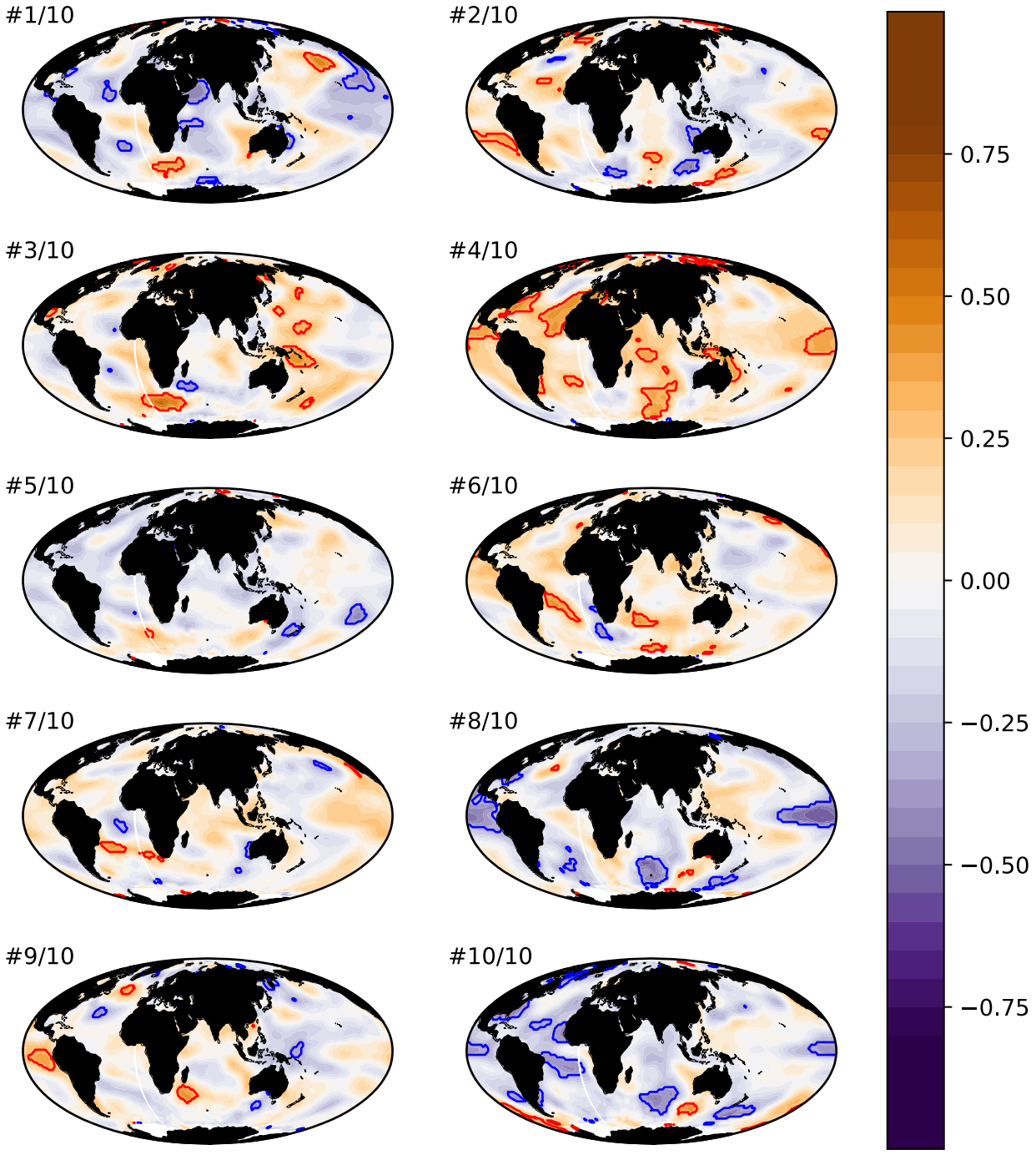

Supplementary Figure 10 | As Fig. 8 but for the austral winter season (JJAS).

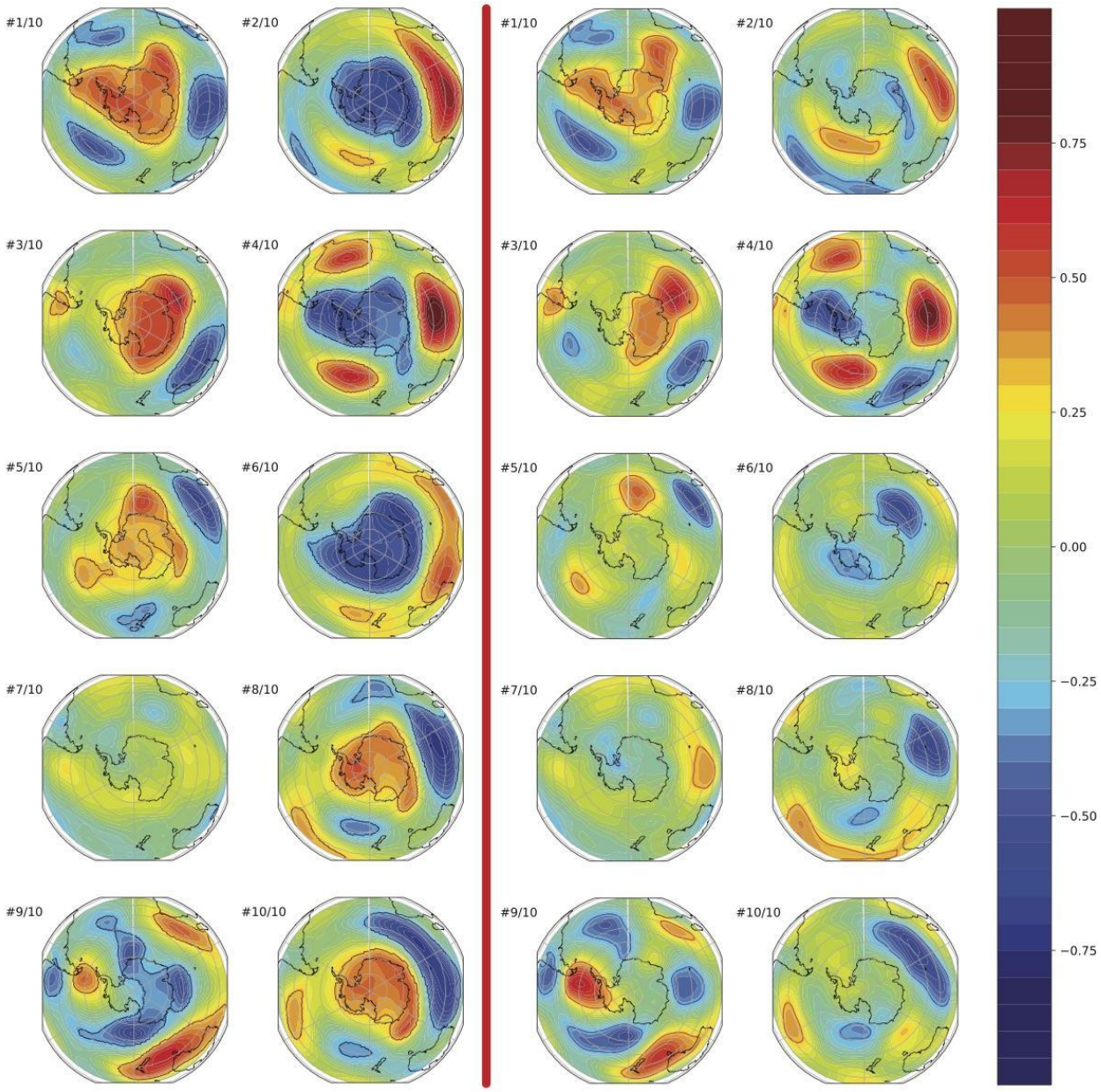

Supplementary Figure 11 | As Fig. 9 but for the austral winter season (JJAS).

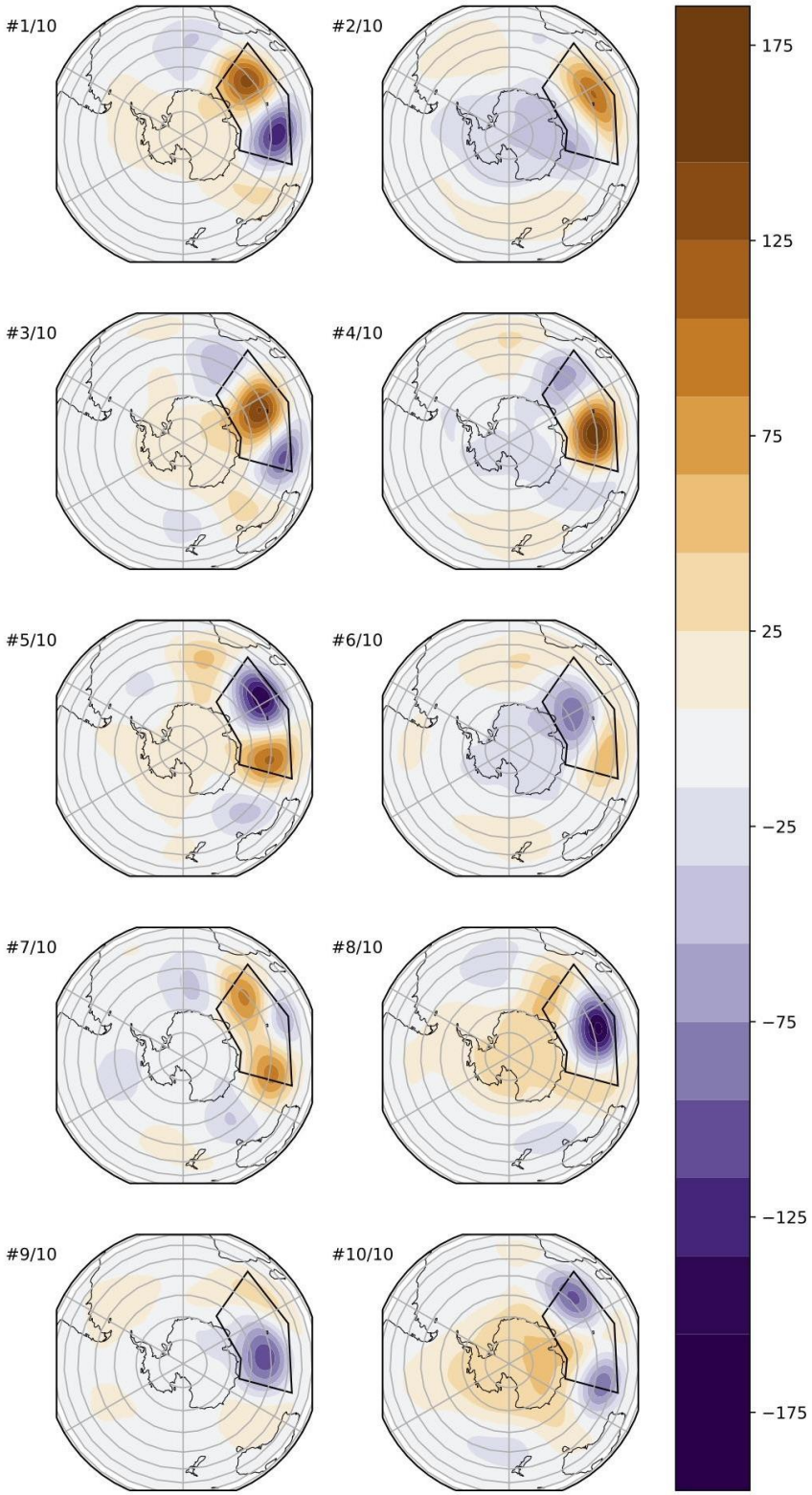

Supplementary Figure 12 | Z_{700} anomaly patterns associated with the 10 weather regimes, period 1979-2018 (m, see color legend). Anomalies that are not significantly different from the mean climatology according to a t-test at the 95% confidence level are shaded white or omitted.

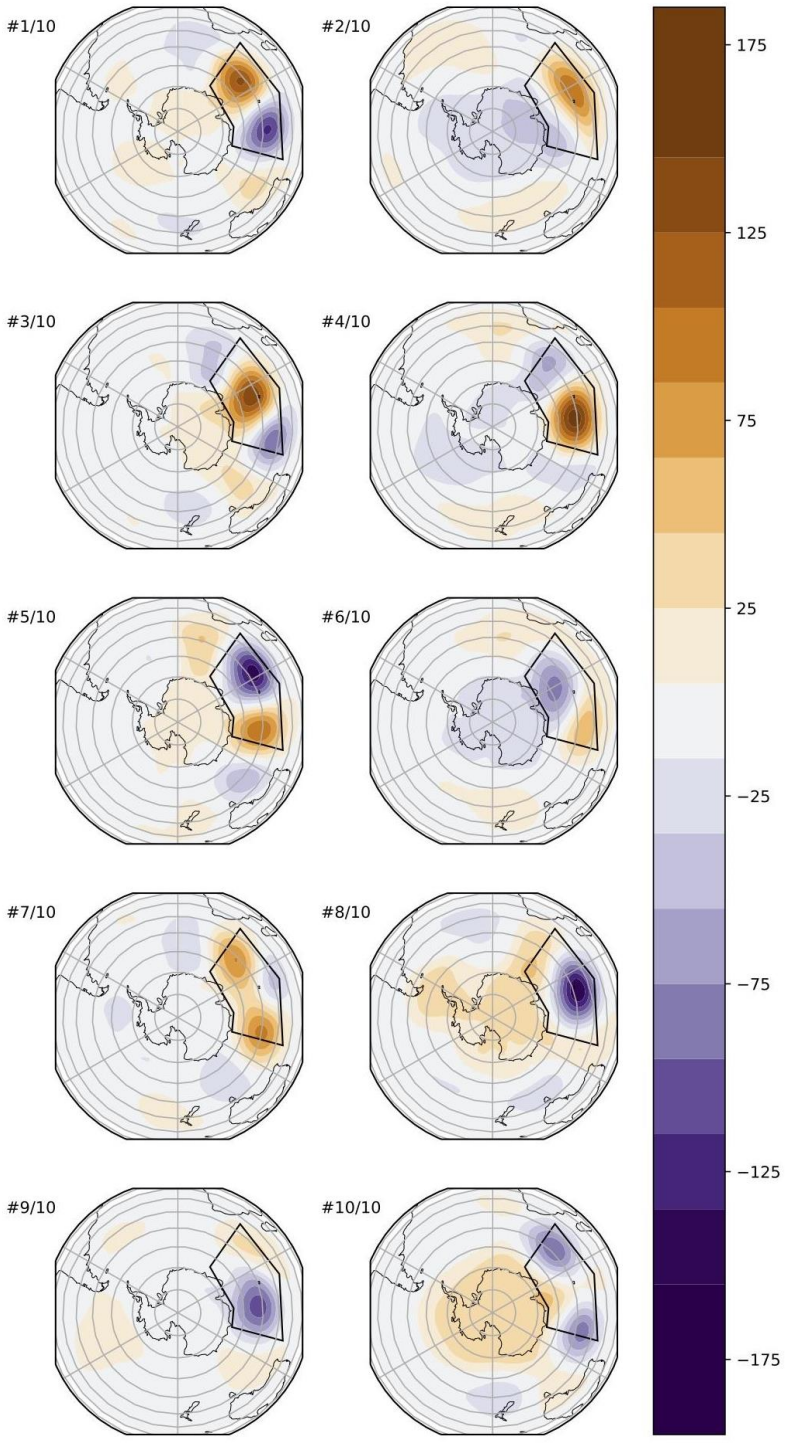

Supplementary Figure 13 | As Supp. Fig. 12 but for the austral summer season (NDJF).

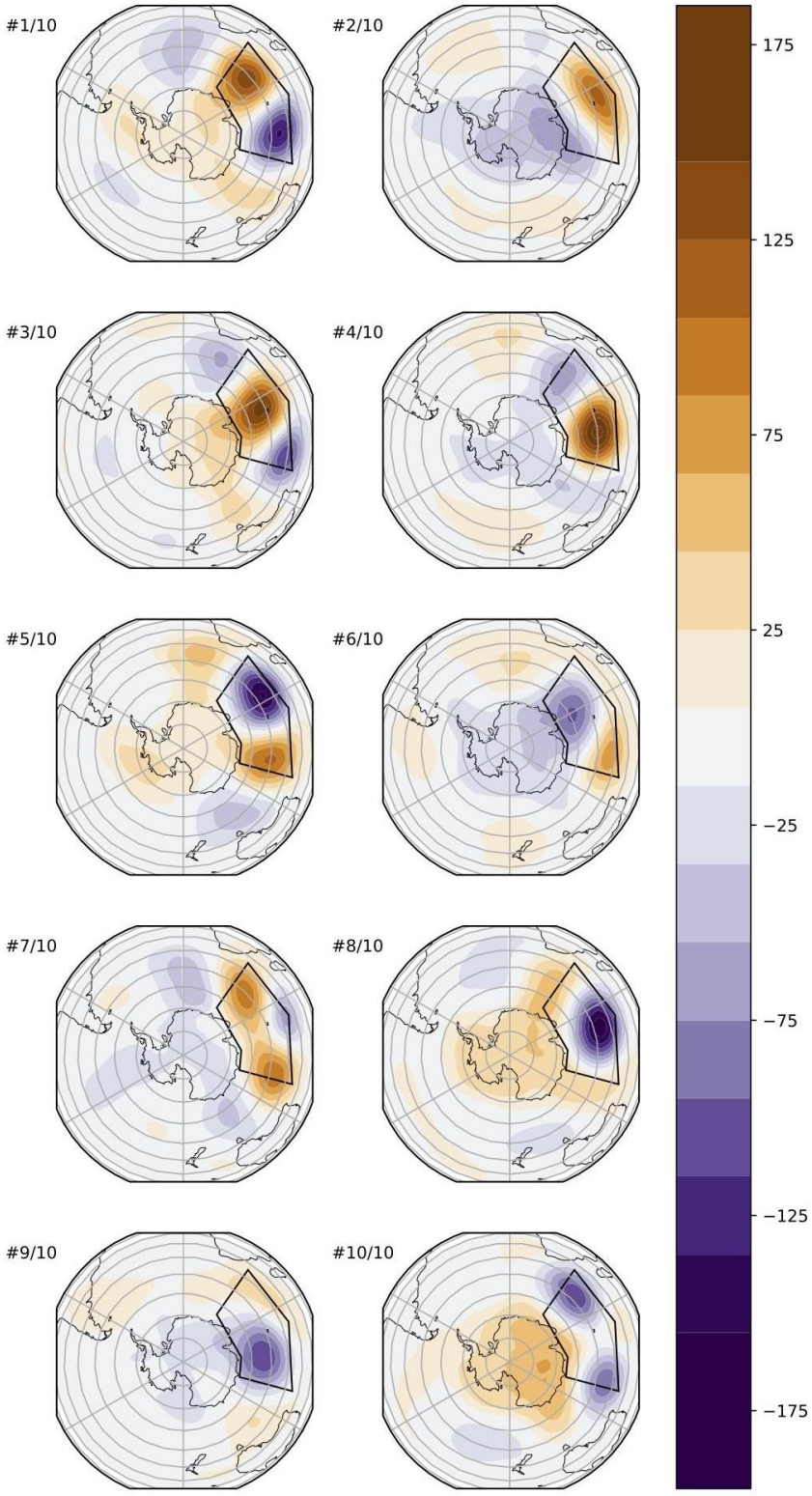

Supplementary Figure 14 | As Supp. Fig. 12 but for the austral winter season (JJAS).

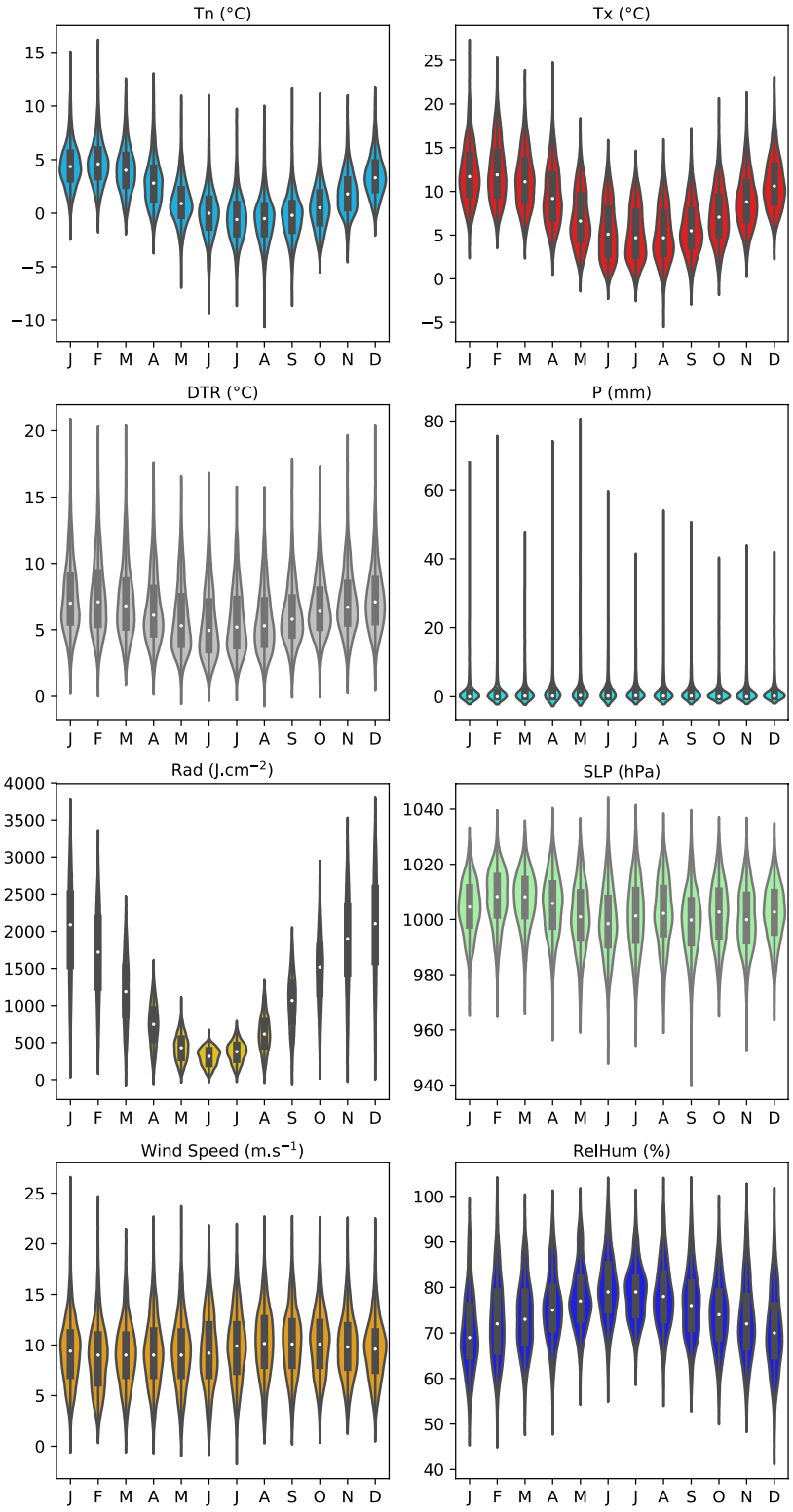

Supplementary Figure 15 | Mean climatology and daily variability recorded at the Port-aux-Français synoptic weather station. The violin plots show the statistical distribution of each variable during each month of the year, period 1979-2018. Violin plot representation is as for Fig. 10.

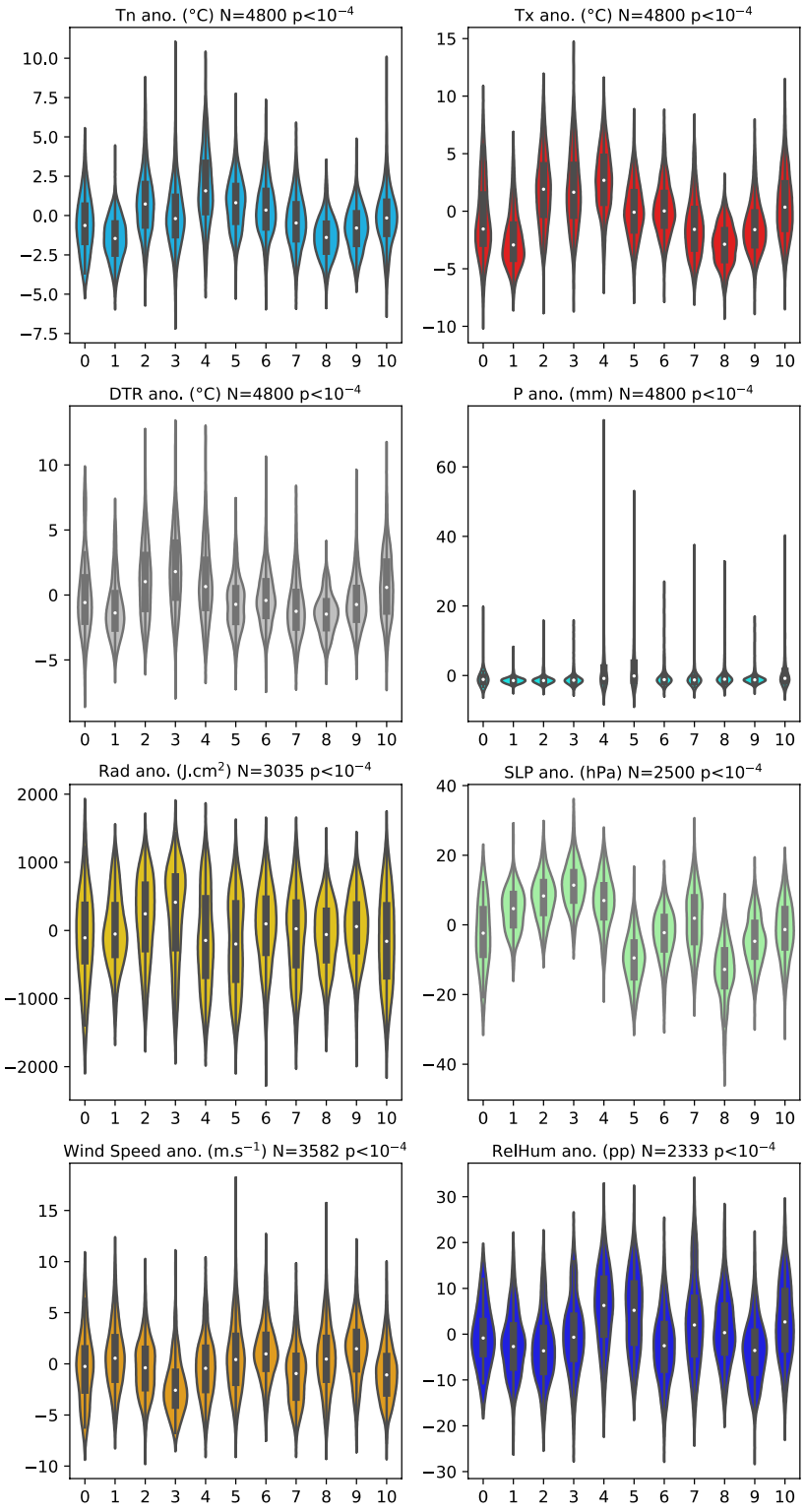

Supplementary Figure 16 | As Fig. 12 but for the austral summer season (NDJF).

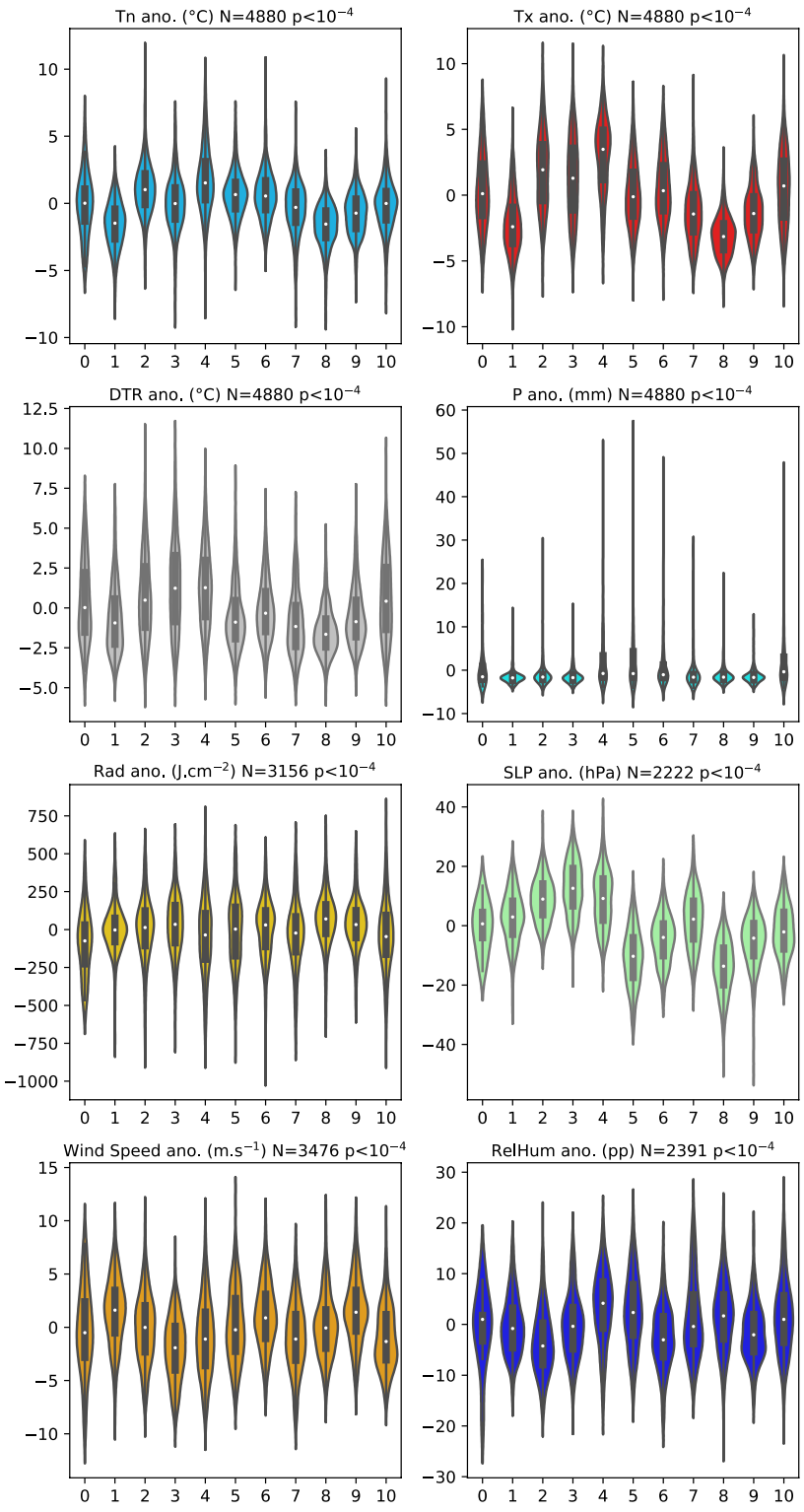

Supplementary Figure 17 | As Fig. 12 but for the austral winter season (JJAS).

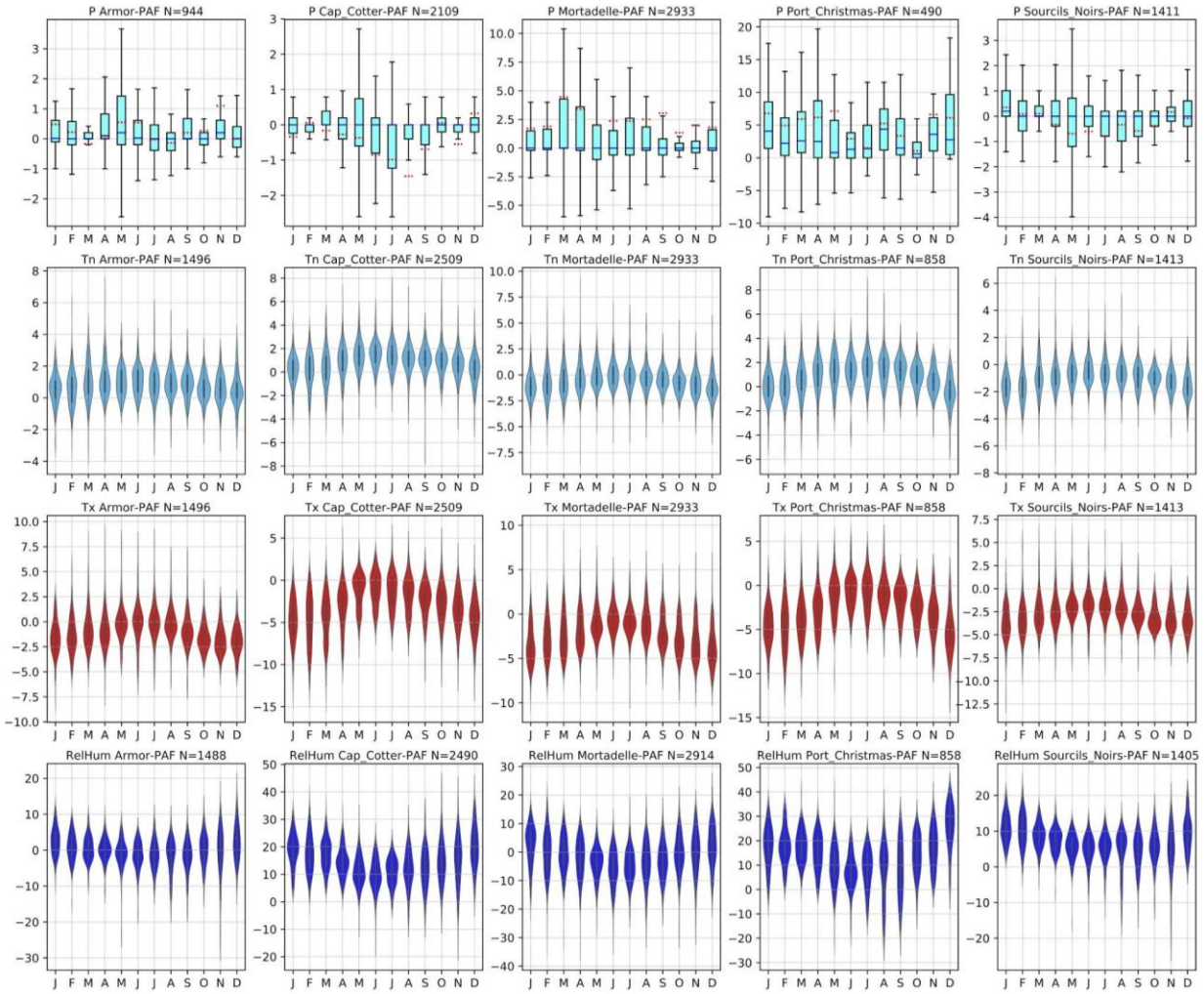

Supplementary Figure 18 | Seasonality in the precipitation (mm: upper row), Tn (°C, second row), Tx (°C, third row) and relative humidity (percentage points, fourth row) time series collected at the 5 Kerguelen weather stations (Armor, Cap Cotter, Mortadelle, Port Christmas and Sourcils Noirs), period February 2012 to December 2018. The number of daily data included in each analysis is labeled in each panel title. Boxplot representation as in Figure 4, with outliers omitted for readability. Violin plot representation, sample construction and statistical significance as in Fig. 10.

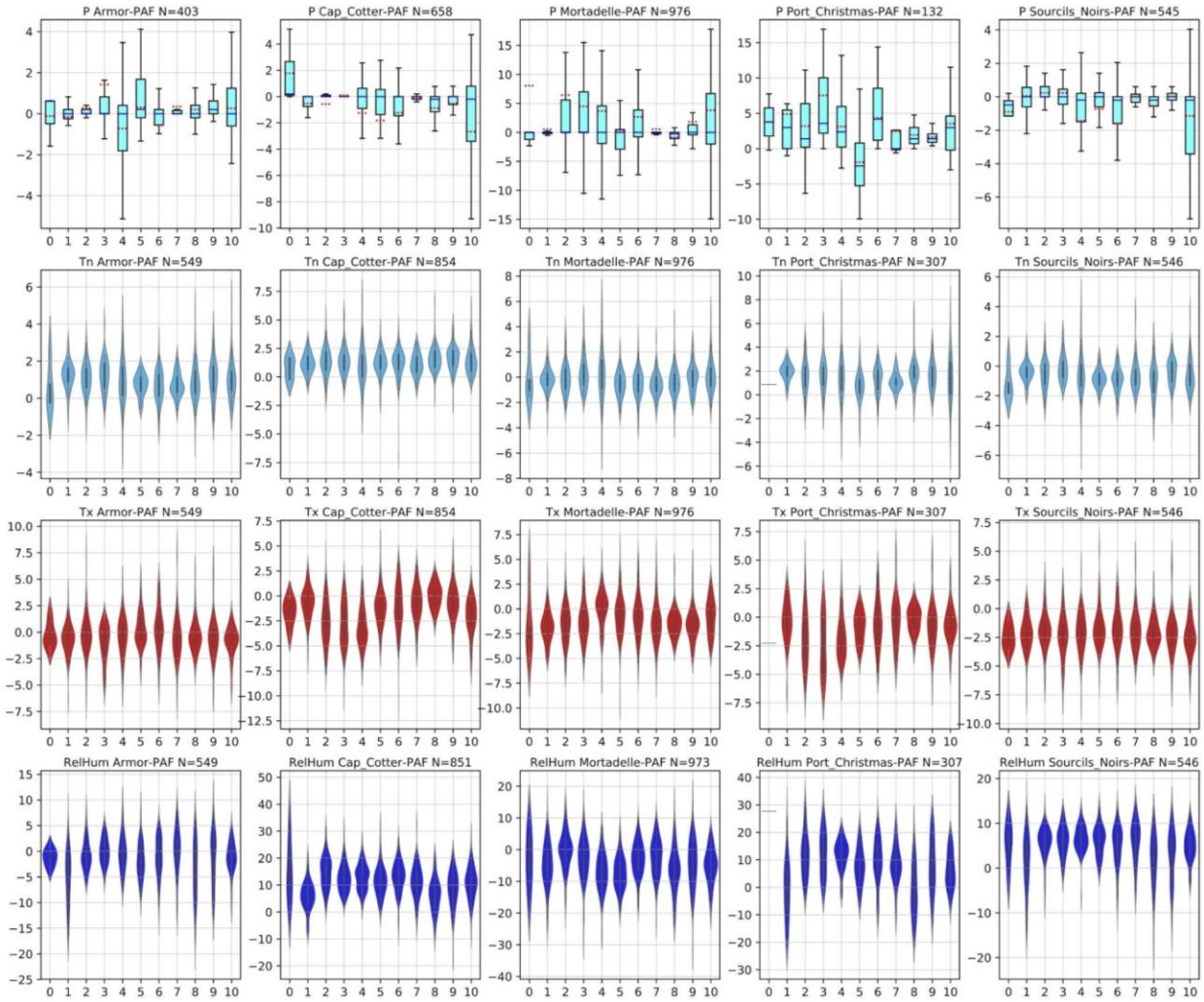

Supplementary Figure 19 | As Fig. 14 but for the austral winter season (JJAS).

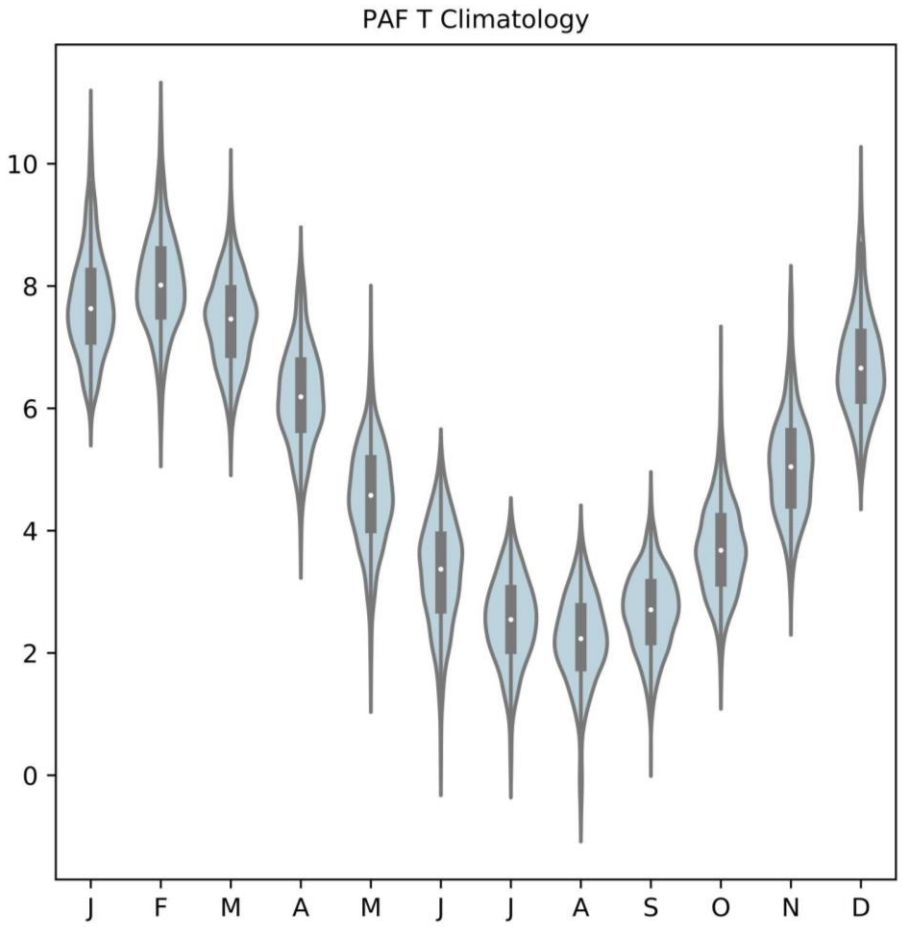

Supplementary Figure 20 | As Supp. Fig. 15 but for water temperature (°C) measured at the tide gauge of the Port-aux-Français station.

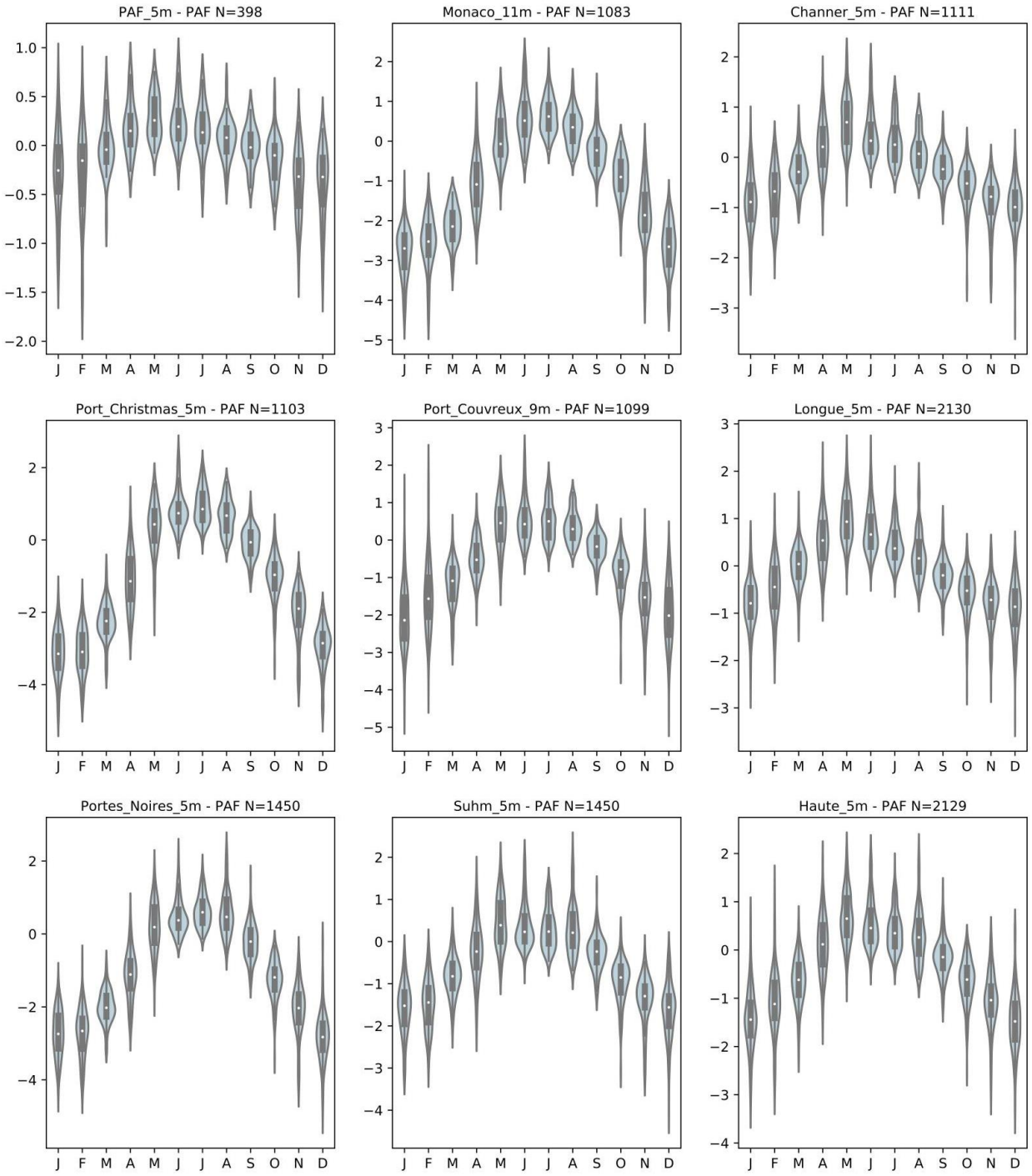

Supplementary Figure 21 | Seasonality in the daily differences in water temperature (°C) between Kerguelen ocean data loggers and Port-aux-Français reference tide-gauge time series, period 6 January 2012 to 31 December 2018. The number of data included in each analysis is labeled in each panel title. Violin plot representation, sample construction and statistical significance are as in Fig. 10.

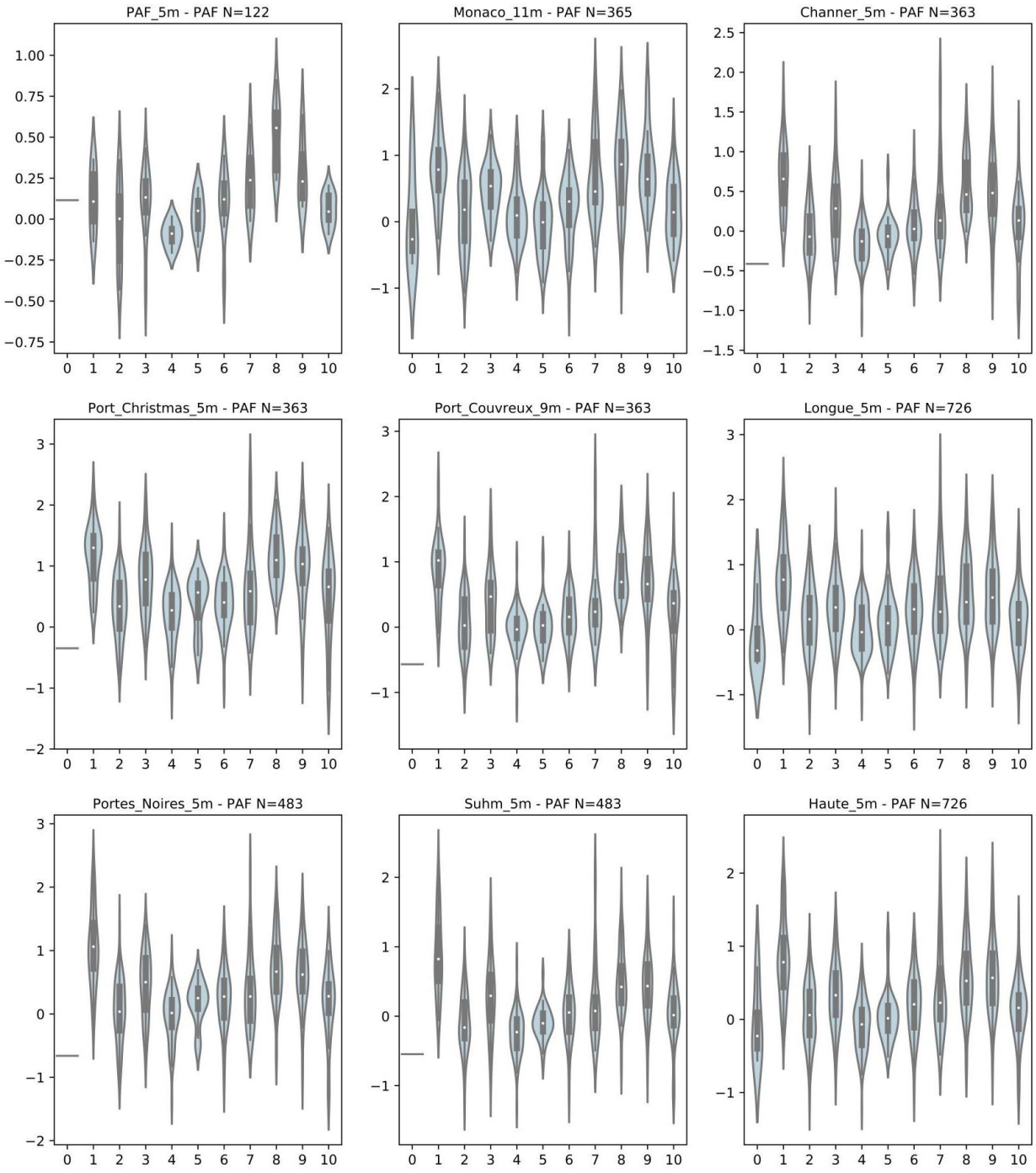

Supplementary Figure 22 | As Fig. 16 but for the austral winter season (JJAS).